


RESEARCH

Open Access



Pretargeted brain PET imaging reveals amyloid- β pathology using a TCO-modified antibody and a fluorine-18-labeled tetrazine

Sara Lopes van den Broek¹, Jonas Eriksson^{2,3}, Qiaojun Yang¹, Nadja M. Bucher¹, Eva Schlein¹, Lorenzo J. I. Balestri², Luke R. Odell², Dag Sehlin¹ and Stina Syvänen^{1*} 

Abstract

Background Antibody-based positron emission tomography (PET) imaging holds great promise for visualizing disease-related proteins in the brain. However, its clinical utility is limited by poor antibody penetration across the blood–brain barrier (BBB) and the requirement for long-lived radionuclides due to slow antibody pharmacokinetics. Pretargeted imaging strategies, in which antibody administration and radioligand injection are separated in time, enable the use of short-lived, high-resolution PET-compatible radionuclides such as fluorine-18.

Methods A bispecific antibody, Bapi-Fab8D3, which targets both amyloid beta ($A\beta$) and the transferrin receptor (TfR) for TfR-mediated transport across the BBB, was conjugated with trans-cyclooctene (TCO) to enable in vivo click chemistry. Following antibody administration to Alzheimer's disease (AD) model mice and sufficient time for accumulation at intrabrain $A\beta$ deposits, a fluorine-18-labeled tetrazine was injected to react in vivo with the TCO handles on the antibody. PET imaging, autoradiography, ex vivo quantification, and histological analyses were performed to evaluate the specificity and distribution of the imaging signal.

Results Bapi-Fab8D3 retained its binding affinity for both $A\beta$ and TfR after TCO-conjugation. In brain sections, reactive TCOs were detected up to three days after antibody injection, indicating successful transcytosis across the BBB and stable target engagement. Pretargeted PET imaging after fluorine-18-labeled tetrazine injection revealed significantly higher signals in AD mice that received TCO-Bapi-Fab8D3 compared to wild-type controls or AD mice that received the unmodified antibody. The uptake pattern corresponded to $A\beta$ plaque distribution, and quantitative analysis showed increased signal in AD-relevant brain regions including the hippocampus and thalamus.

Conclusions This study demonstrates successful pretargeted PET imaging of brain $A\beta$ pathology using a systemically administered bispecific antibody capable of BBB penetration and a fluorine-18-labeled tetrazine. These findings establish a generalizable strategy for high-contrast in vivo imaging of brain protein targets using pretargeted PET, with the potential to expand molecular imaging to protein targets in the brain that are currently inaccessible.

Keywords Pretargeted PET imaging, Blood–brain barrier, Bispecific antibody, Amyloid- β , Fluorine-18 tetrazine

*Correspondence:

Stina Syvänen

stina.syvanen@uu.se

Full list of author information is available at the end of the article



© The Author(s) 2025. **Open Access** This article is licensed under a Creative Commons Attribution 4.0 International License, which permits use, sharing, adaptation, distribution and reproduction in any medium or format, as long as you give appropriate credit to the original author(s) and the source, provide a link to the Creative Commons licence, and indicate if changes were made. The images or other third party material in this article are included in the article's Creative Commons licence, unless indicated otherwise in a credit line to the material. If material is not included in the article's Creative Commons licence and your intended use is not permitted by statutory regulation or exceeds the permitted use, you will need to obtain permission directly from the copyright holder. To view a copy of this licence, visit <http://creativecommons.org/licenses/by/4.0/>. The Creative Commons Public Domain Dedication waiver (<http://creativecommons.org/publicdomain/zero/1.0/>) applies to the data made available in this article, unless otherwise stated in a credit line to the data.

Background

With an ageing population, the prevalence of neurodegenerative diseases is expected to rise significantly. Currently, treatment options remain limited, with most available drugs targeting symptoms rather than the underlying causes of these diseases. However, a promising therapeutic strategy that has emerged over the past decades is immunotherapy [1, 2]. Notably, the recently approved antibody lecanemab targets amyloid- β ($A\beta$) in the brains of Alzheimer's disease (AD) patients, facilitating its clearance. The approval of lecanemab (NCT03887455), and the ongoing clinical evaluations (NCT04437511, NCT02484547, NCT04639050) of similar antibodies expected to gain approval in the coming years, have been greatly supported by positron emission tomography (PET) imaging of aggregated $A\beta$ in the brain. PET imaging has convincingly demonstrated that these antibodies reduce brain levels of insoluble $A\beta$, i.e., plaques [3, 4]. Despite its value, PET imaging of aggregated proteins is currently limited to detecting amyloids, the characteristic β -sheet structure found in deposits of densely packed $A\beta$ fibrils [5, 6]. It is important to note that amyloid-PET is not specific to the $A\beta$ protein, as other proteins can also form amyloid structures. Moreover, antibodies such as lecanemab target a range of soluble and diffuse $A\beta$ aggregates, rather than the amyloid core of plaques. This creates a partial mismatch between the therapeutic target of immunotherapy and the structures visualized using amyloid PET imaging. For other neurodegenerative diseases characterized by pathological protein aggregation, such as those involving alpha-synuclein, TAR DNA-binding protein 43, or proteins related

to neuroinflammation, there are currently either suboptimal or no effective PET radioligands available. Developing small molecule-based PET ligands for these proteins has proven challenging due to off-target binding and poor imaging contrast [7–10].

An alternative approach to small molecule-based PET ligands involves radiolabeling antibodies or antibody fragments for use as PET radioligands. Antibodies offer high target specificity, but suffer from poor brain delivery and long circulation times, which limit their use as radioligands in PET imaging. To overcome the low brain delivery, bispecific antibody formats have been engineered by fusing a transferrin receptor (TfR)-binding domain to the primary antibody. The TfR serves as a shuttle, significantly enhancing antibody transport across the blood–brain barrier (BBB) [11–15]. Nonetheless, the long systemic half-life of antibodies remains a significant hurdle for antibody-based PET, as it necessitates imaging several days after administration to allow clearance of background signal from circulating radiolabeled antibodies. Additionally, it requires the use of long-lived radionuclides, such as iodine-124 or zirconium-89, which results in relatively high radiation doses to patients. Clinically, it would be preferable to use fluorine-18 (^{18}F), a radionuclide with a half-life of just under two hours.

In addition to its short half-life, ^{18}F emits positrons with low kinetic energy and has a high positron emission fraction, which contribute to high-resolution images and lower radiation burden. To enable antibody-based PET imaging with ^{18}F , the pretargeted imaging concept has been proposed (Fig. 1) [16–19]. In this strategy, the antibody is modified with a reactive

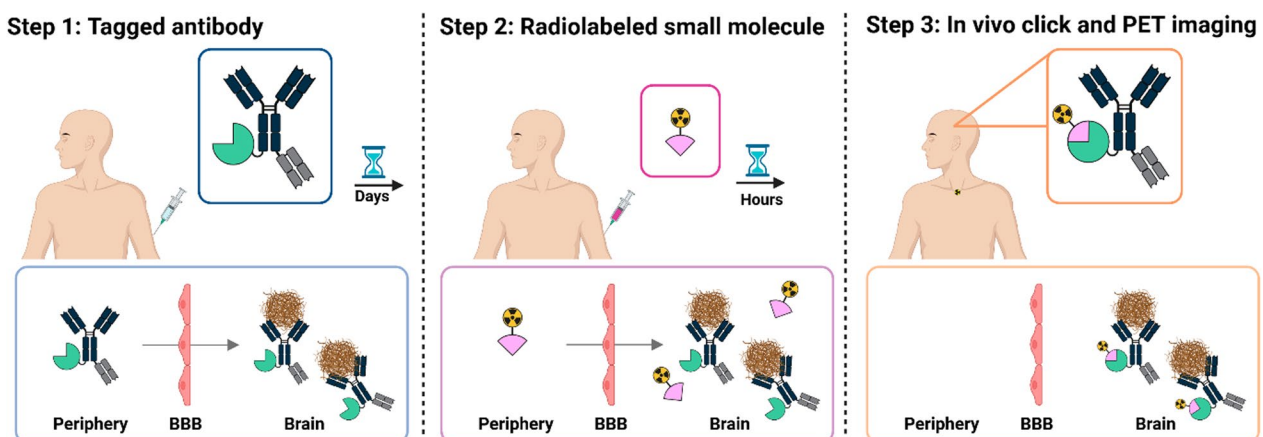


Fig. 1 Overview of pretargeted PET imaging with brain-penetrant antibodies. In pretargeted PET imaging using bispecific brain-penetrant antibodies, Step 1 involves modifying the antibody with a reactive “handle” prior to administration. After injection, the antibody crosses the blood–brain barrier (BBB), binds to its target protein (in this study amyloid- β), and is given time to clear from the circulation. Step 2 consists of administering a small molecule carrying the radionuclide (in this study fluorine-18) and a complementary reactive group. This radiolabeled molecule rapidly reacts with the antibody’s handle at the target site, thereby labelling the target protein in vivo. Step 3 occurs once the unbound radiolabeled molecule has cleared, at which point PET imaging is performed to visualize the labeled target. Illustrations were created with BioRender.com

“handle” (e.g., trans-cyclooctene, TCO) but is not radiolabeled prior to administration. After administration, the antibody binds to its target protein and is given time to clear from circulation without concerns related to radioactive decay or patient radiation dose. At the optimal time point, defined by high target engagement and low systemic antibody levels, a small molecule carrying the radionuclide and a complementary reactive group (e.g., a tetrazine) is administered. This radiolabeled molecule rapidly reacts with the antibody’s handle at the target site, effectively labelling the target protein of interest in vivo [19–21].

In this study, we establish a robust and versatile platform for pretargeted brain PET imaging by combining TCO-modified bispecific antibodies capable of TfR-mediated brain delivery with ^{18}F -labeled tetrazines for rapid in vivo click chemistry. By leveraging the high specificity and efficiency of the tetrazine ligation reaction, we demonstrate specific visualization of brain A β pathology. Importantly, while this work focuses on A β , the strategy can be readily adapted to a wide range of brain targets, enabling the imaging of diverse pathologies in both research and clinical settings, provided that a suitable antibody is available.

Materials and methods

Animals

All ex vivo biodistribution and PET imaging studies were performed in old (12–19 months) in-house-bred App^{NL-G-F} knock-in mice, expressing mouse amyloid precursor protein (*APP*) with a humanized A β sequence as well as the Swedish (KM670/671NL), Arctic (E693G) and Beyreuter/Iberian (I716F) mutations, leading to rapid pathology progression [22]. Age-matched wild-type (WT) mice (C57BL/6J BomTac) were used as a control. Ex vivo pretargeting experiments also included in-house-bred Tg-ArcSwe mice, a transgenic model that harbors the Swedish and the Arctic APP mutations and is characterized by high levels of aggregated A β that forms dense-core plaques [23, 24]. To study brain distribution of an assumingly non-brain penetrant tetrazine (later used for blocking peripheral TCO groups), 4-month-old WT mice were used. Both males and females were included in all studies (Table S1). The mice were housed in an approved animal facility at Uppsala University with ad libitum access to food and water. All described procedures were approved by the Uppsala Country Animal Ethics board (5.8.18–16493/2024) following the legislation and regulations of the Swedish Animal Welfare Agency and European Communities Council Directive of 22 September 2010 (2010/63/EU).

Antibody modifications

The bispecific antibody Bapi-Fab8D3 is derived from the full-length IgG antibody bapineuzumab (Bapi), which targets the N-terminus of A β and has previously been investigated as an anti-A β therapeutic [25]. An Fab fragment of the murine TfR-binding antibody 8D3 (Fab8D3) was fused to the C-terminus of one of the Bapi heavy chains, resulting in a bispecific format. Mutations (L234A, L235A, P329G) were introduced to the Fc-domain to reduce effector functions [26, 27]. This design closely resembles the BrainShuttle format developed by Roche [28, 29]. Bapi-Fab8D3 was transiently expressed in Expi293F cells (ThermoFisher, Waltham, MA, A14527) following a previously described protocol [30].

Bapi-Fab8D3 was then modified at lysine residues using TCO-NHS ester, following a previously described procedure [16]. Briefly, sodium carbonate buffer (1 M, pH 8.0) was added to phosphate-buffered saline (PBS) containing Bapi-Fab8D3 (1.5–3.0 mg/mL) to achieve a final buffer concentration of 30 mM. Axial TCO-NHS ester (BioNordika, Solna, Sweden, VEC-CCT-1509-25) dissolved in dimethylsulfoxide (DMSO) was then added at a 20–50 molar excess relative to the antibody. The reaction mixture was incubated at 600 rpm for 2 h at room temperature in the dark. Unreacted TCO-NHS ester was subsequently removed using Zeba Spin desalting columns (7 K MWCO, 0.5 mL; ThermoFisher, 89882), and the modified antibody was eluted in PBS (pH 7.4). The final protein concentration was determined using a spectrophotometer (DS-11, DeNovix, Wilmington, DE).

Enzyme-linked immunosorbent assays (ELISA) was used to investigate antibody binding towards A β and murine TfR. The 96-well half-area plates (Corning Inc., New York, NY) were coated overnight at 4 °C with A β (50 nM diluted in PBS), murine TfR (50 μL /well, 5 μg /mL diluted in PBS), or anti-human IgG (hIgG) (0.5 μL /well, 5 μg /mL diluted in PBS). The wells were blocked with 1% bovine serum albumin (BSA) in PBS for 1 h. The antibodies Bapi-Fab8D3 and TCO-Bapi-Fab8D3 variants were serially diluted in incubation buffer (PBS with 0.1% BSA, 0.05% Tween-20 and 0.15% Kathon) from 50 nM to 3.2 pM and incubated for 2 h. The plates were washed with wash buffer and detected with horseradish peroxidase (HRP)-coupled goat hIgG-F(ab')₂ (1:2000, Jackson ImmunoResearch Laboratories, West Grove, PA, 109-036-006). Plates were developed with K blue aqueous TMB substrate (Neogen Corp., Lexington, KY), quenched with 1 M H₂SO₄ and read with a spectrophotometer at 450 nm. The data were corrected for concentration obtained from the hIgG ELISA.

The number of TCOs conjugated per antibody was determined by SDS-PAGE. Aliquots of TCO-Bapi-Fab8D3 in PBS (10 μL , 0.005–0.025 nmol expected

TCO per sample) were mixed with aliquots of CF647-Tetrazine (Bionordika, Solna, Sweden, BIT-96056, 5 μ L, 0.05 nmol) in PBS containing 10% DMSO, ensuring an excess of tetrazine in comparison to TCOs. The samples were mixed and incubated at 600 rpm for 1 h at 37 °C. Bolt Sample Buffer (5 μ L, B0007, Invitrogen, Carlsbad, CA) was added to each sample and the samples were heated to 95 °C and incubated at 600 rpm for 2 min. Samples were applied onto SDS-PAGE gels (Bolt Bis-Tris Plus Mini Protein Gels, 4%–12%, 1.0 mm, 12-well, NW04122BOX, Invitrogen), alongside a molecular weight standard (PageRuler Plus Prestained Protein Ladder, 26619, Invitrogen) and a CF647-Tetrazine control followed by electrophoresis in Bolt MES SDS running buffer (B0002, Invitrogen) for 20 min at 200 V. After electrophoresis, gels were removed from their cassette and directly imaged for AF647-fluorescent intensity using an iBright FL1500 Imaging System (Invitrogen) and fluorescence was quantified according to previously published procedures [16, 17]. After fluorescence quantification, which reflects the number of TCO groups conjugated per antibody based on tetrazine binding, the gel was stained with InstantBlue Coomassie Protein Stain (ab119211, Abcam, Cambridge, UK), and an image was taken with the iBright FL1500 Imaging System.

Radiochemistry

Synthesis of [^{68}Ga]Ga-DOTA-PEG₁₁-Tz

To investigate the reactivity of TCO groups after in vivo accumulation in the brain, the polar tetrazine DOTA-PEG₁₁-Tz (Fig. S1a) was selected for incubation with brain sections prepared from mice administered with TCO-Bapi-Fab8D3. This tetrazine was radiolabeled with gallium-68 (^{68}Ga) to enable detection by autoradiography, following the protocol described below.

[^{68}Ga]GaCl₃ (329 MBq) in 0.1 M HCl (1.3 mL) was added to a reaction vial containing DOTA-PEG₁₁-Tz (50–100 μ g, 0.04–0.08 μ mol) in ammonium acetate buffer (0.2 M, pH 7, 40 μ L), 70% ethanol (400 μ L), and additional ammonium acetate buffer (0.2 M, pH 6, 1000 μ L). The reaction mixture was heated at 90 °C for 10 min, then purified using a solid-phase extraction (SPE) cartridge (Sep-Pak Plus Light C18, WAT036805, Waters, Milford, MA), which had been pre-conditioned with 70% ethanol (2.5 mL) and water (5 mL). The SPE cartridge was washed with water (5 mL), and the product was eluted with ethanol (1 mL), yielding [^{68}Ga]Ga-DOTA-PEG₁₁-Tz with a decay-corrected radiochemical yield (RCY) of 66% corresponding to 179 MBq (non-decay-corrected RCY of 54%). Radiochemical purity (RCP) was assessed by radio-thin layer chromatography (radio-TLC) using silica gel 60 plates (1.05554.0001, Merck) and citrate buffer (0.1 M, pH 4) as the mobile phase. The retention factors

(Rf) were: [^{68}Ga]Ga-DOTA-PEG₁₁-Tz: Rf=0; free [^{68}Ga]GaCl₃: Rf=1. The RCP was >98%, and the molar activity (Am) was 5.7 GBq/ μ mol.

Synthesis of ^{18}F -labeled tetrazines

For in vivo pretargeted imaging, two brain-penetrant tetrazines were used, [^{18}F]HTzA and [^{18}F]MeTzA (Fig. S1b, c). The labeled tetrazines were synthesized as previously described [31, 32], providing [^{18}F]MeTzA with a Am of 109 ± 5 GBq/ μ mol, a radioactivity yield of 1380 ± 260 MBq, and a RCP of $97.5\% \pm 1.5\%$ ($n=4$). [^{18}F]HTzA was synthesized accordingly, affording the labeled tetrazine with a Am of 123 ± 34 GBq/ μ mol, a radioactivity yield of 830 ± 150 MBq, and a RCP of $98.0\% \pm 1.0\%$ ($n=5$).

Ex vivo pretargeted imaging

App^{NL-G-F}, Tg-ArcSwe and WT mice ($n=6$ in total, $n=1$ per group) were intravenously (i.v.) injected with 20 nmol/kg Bapi-Fab8D3 or TCO-Bapi-Fab8D3 via the tail vein. This dose was selected based on previous studies, with the aim of achieving high brain concentrations without blocking TfR-mediated transcytosis [33]. Three days later, mice were anesthetized with isoflurane, followed by transcardial perfusion with 0.9% NaCl to remove blood. In parallel, App^{NL-G-F}, Tg-ArcSwe and WT mice ($n=3$ in total, $n=1$ per group) that did not receive antibody were perfused as additional controls. Brains were isolated and divided into the left and right hemispheres, and immediately frozen. Sagittal brain sections (20 μ m, $n=6$ per brain) between 1.2 and 2.2 mm lateral to the midline were prepared using a Cryostar NX70 (ThermoFischer). The sections were then incubated with [^{68}Ga]Ga-DOTA-PEG₁₁-Tz (20 nM in PBS-0.1% Tween20) for 45 min at room temperature. Afterwards, sections were washed in cold PBS (3 \times 3 min) and cold water (1 \times 1 min). After drying, sections were exposed to a phosphor imaging plate (BAS-IP SR 2040, Fujifilm, 28956477) for 2.5 h and the plate was scanned in an Amersham Typhoon IP phosphor imager (GE Healthcare, 29187194) at a resolution of 50 μ m. To visualize the distribution of A β pathology, brain sections from separate App^{NL-G-F}, Tg-ArcSwe and WT mice were stained with Luminescent Conjugated Oligothiophene (LCO) HS-84 according to a previously published procedure [34].

PET imaging

Selection of [^{18}F]tetrazine

To investigate and compare the pharmacokinetics of the two tetrazines, [^{18}F]HTzA (10.4 ± 4.4 MBq) and [^{18}F]MeTzA (12.9 ± 4.5 MBq) were intravenously injected into App^{NL-G-F} and WT mice. A 90-min PET scan (Mediso NanoPET/MR, Mediso Medical Imaging

System, Hungary) was initiated at the time of injection, followed by a 5-min computed tomography (CT) scan (Mediso NanoSPECT/CT, Mediso Medical Imaging System). Anesthesia was maintained throughout the scanning procedure using 3.5%–4.0% sevoflurane in a 0.5 L/min flow of 50% oxygen and 50% medical air. After the CT scan, the animals were returned to their home cages. At 3.5 h post-radioligand administration, the mice were again anesthetized and subjected to a 60-min PET scan, followed by an additional CT scan. At 5 h post-injection, a terminal blood sample was obtained from the heart before the mice were perfused, and the brain and peripheral organs were collected. Radioactivity in the tissues was quantified via γ -counting using a 2480 Wizard automatic gamma counter (PerkinElmer). PET data were reconstructed on a $160 \times 160 \times 128$ grid with voxel dimensions of $0.5 \times 0.5 \times 0.6$ mm³ using three-dimensional ordered-subsets expectation maximization (20 iterations). CT data were reconstructed using filtered back-projection. PET and CT images were processed using the PMOD image analysis software (PMOD Technologies, Zurich, Switzerland, version 4.105). PET images were co-registered to the corresponding CT scans, and the CT images were manually aligned to a standard brain atlas using the Fuse module. Volumes of interest (VOIs) were defined based on this alignment and applied to the dynamic PET data.

All measured activity concentrations, obtained either by PET imaging or γ -counting, were converted to standardized uptake values (SUV). SUV is a dose- and body weight-normalized measure of radioligand concentration that enables comparison between subjects administered with different amounts of radioactivity and between individuals with varying body weights. SUV was calculated as follows: $SUV = \text{Tissue radioactivity concentration (Bq/mL)} / \text{Injected activity (Bq) per body weight (g)}$.

In vivo brain delivery of [⁶⁸Ga]Ga-DOTA-PEG₁₁-Tz

DOTA-PEG₁₁-Tz, previously used to determine reactivity of TCO groups on brains sections, was also investigated as an agent to block TCO groups on TCO-Bapi-Fab8D3 present in the circulation to avoid them reacting with the brain penetrant [¹⁸F]tetrazines used for pretargeting. For this, it was crucial to ensure that the DOTA-PEG₁₁-Tz did not enter the brain as this could reduce the number of available TCO for the pretargeted PET. Hence, 4-month-old WT mice received i.v. ($n=6$) or intraperitoneal (i.p.) ($n=3$) injection of 5.6 ± 1.8 MBq [⁶⁸Ga]Ga-DOTA-PEG₁₁-Tz. The i.v. administered animals were euthanized after perfusion at 3 min or 6 h, while the i.p. administered animals were euthanized at 6 h. Radioactivity in the brain was quantified via γ -counting.

Pretargeted imaging

To evaluate pretargeted imaging, mice received either Bapi-Fab8D3 or TCO-Bapi-Fab8D3 at a dose of 20 nmol/kg three days before PET scanning. On the day of scanning, the non-brain-penetrant tetrazine DOTA-PEG₁₁-Tz was administered i.p. at a dose of 100 nmol/kg to block TCO groups on TCO-Bapi-Fab8D3 present in the blood circulation. This dose corresponded to a fivefold molar excess relative to the administered TCO dose, and likely represented approximately a 100-fold molar excess compared to the amount of TCOs remaining in circulation three days after TCO-Bapi-Fab8D3 injection. Two hours later, the animals were positioned in the PET scanner, injected with 13.2 ± 3.7 MBq of [¹⁸F]HTzA, and scanned for 90 min, followed by a 5-min CT scan. As in the tetrazine-only protocol, the mice were returned to their home cages and rescanned at 3.5 h post-radioligand administration. A subset of animals did not undergo the initial 90-min scan but were scanned only at the 3.5-h time point. These mice remained anesthetized during the first 90 min to match the experimental conditions of the group that also received an early scan. Brain, terminal blood and organ isolation, as well as image post-processing, were conducted as described in the previous section.

Quantification of brain A β

The cerebrum of the left hemisphere isolated from PET-scanned animals was homogenized with a Precellys Evolution (Bertin Technologies, Montigny-le-Bretonneux, France) (4×10 s at 5500 rpm) at a 1:5 weight/volume ratio in Tris-buffered saline (TBS) with 1% complete protease inhibitor (Sigma). After centrifugation for 1 h at $16,000 \times g$, the supernatant was immediately removed and frozen. Pellets were dissolved in 70% formic acid (FA) and centrifuged at $16,000 \times g$ for 1 h followed by supernatant collection. Concentrations of A β 38, A β 40, and A β 42 in FA-extracted brain homogenate was quantified using the V-PLEX[®] A β peptide panel 1 (6E10) immunoassay (Meso Scale Discovery, Rockville, MD, K15200E). Samples were neutralized with 2 M Tris and diluted in assay diluent (1:10,000) before being loaded in duplicate onto pre-coated and blocked 96-well plates together with the secondary A β antibody 6E10 conjugated to a SULFO-TAG for electro-chemiluminescent detection. After 2 h of incubation, plates were washed with PBS containing 0.05% Tween, and Meso Scale Discovery read buffer was added. Plates were read with a MESO QuickPlex SQ instrument (Meso Scale Discovery).

Statistics

Data are presented mean \pm standard deviation (SD). One-way ANOVA followed by Tukey's multiple comparisons

test or two-way ANOVA followed by Šídák's multiple comparisons test was used to correct for multiple comparisons. All tests were two-tailed, with a significance level set at 95%. $P < 0.05$ was considered as statistically significant. Graphs and statistical analyses were performed using GraphPad Prism version 10.4.2 (GraphPad Software, San Diego, CA).

Results

Affinity is preserved after TCO-modification

The bispecific antibody Bapi-Fab8D3, in which the Bapi domain targets A β and the Fab8D3 domain binds to the murine TfR, was modified with varying molar excess of TCO over antibody. Modification with 20 and 50 molar equivalents of TCO resulted in the conjugation of an approximate average of 6 and 9 TCO moieties per Bapi-Fab8D3 molecule, respectively. Affinity towards both targets, A β and TfR, was preserved with both modifications (Fig. 2a, b). Therefore, the Bapi-Fab8D3 modified with 50 equivalents of TCO was selected for subsequent experiments.

TCO-Bapi-Fab8D3 accumulates at A β aggregates with reactive TCOs at 3 days post administration

To assess the in vivo reactivity of the TCO groups, TCO-Bapi-Fab8D3 was administered to two mouse models expressing A β pathology (App^{NL-G-F} and Tg-ArcSwe), as well as to WT control mice in an exploratory, qualitative experiment. For comparison, the unmodified Bapi-Fab8D3 was also administered. Three days post-injection, brains were collected and sagittal sections were prepared from the right hemisphere. As additional controls, brain sections were also obtained from mice that had not received any antibody. After incubation with the highly polar and reactive [⁶⁸Ga]Ga-DOTA-PEG₁₁-Tz,

the sections were subjected to autoradiography. Sections from App^{NL-G-F} and Tg-ArcSwe mice that had received TCO-Bapi-Fab8D3 exhibited a clear autoradiographic signal, indicating that the antibody successfully crossed the BBB, bound to A β aggregates, and crucially, that TCO groups remained reactive after in vivo administration and target binding (Fig. 3a). In contrast, no specific signal was observed in sections from WT mice injected with TCO-Bapi-Fab8D3, mice injected with unmodified Bapi-Fab8D3, or non-injected controls (Fig. 3a). The spatial distribution of the signals detected by autoradiography in App^{NL-G-F} and Tg-ArcSwe mice that had received TCO-Bapi-Fab8D3 injection corresponded to brain regions typically containing high levels of A β [35, 36] as shown by LCO staining of A β deposits (Fig. 3b–d). While the App^{NL-G-F} mice exhibited widespread A β pathology, the Tg-ArcSwe mice displayed somewhat less extensive pathology, with particularly low levels in the cerebellum, a region that is less affected in this model.

Brain pharmacokinetics and systemic elimination of two ¹⁸F-labeled tetrazines

For in vivo imaging using the pretargeted approach, the radiolabeled tetrazine should ideally enter the brain rapidly, and unbound (non-reacted) tetrazine should display efficient clearance from the brain and be eliminated from the blood quickly to allow for high imaging contrast. Two tetrazines, MeTzA and HTzA, radiolabeled with the clinically preferred radionuclide ¹⁸F, were evaluated in App^{NL-G-F} and WT mice. Both tetrazines exhibited rapid brain entry, reaching peak concentrations within 5 min post administration. The [¹⁸F]MeTzA showed higher peak brain uptake than [¹⁸F]HTzA (Fig. 4a). At 4 h post-injection, brain concentrations measured in vivo by PET were similar for both tetrazines, with no significant

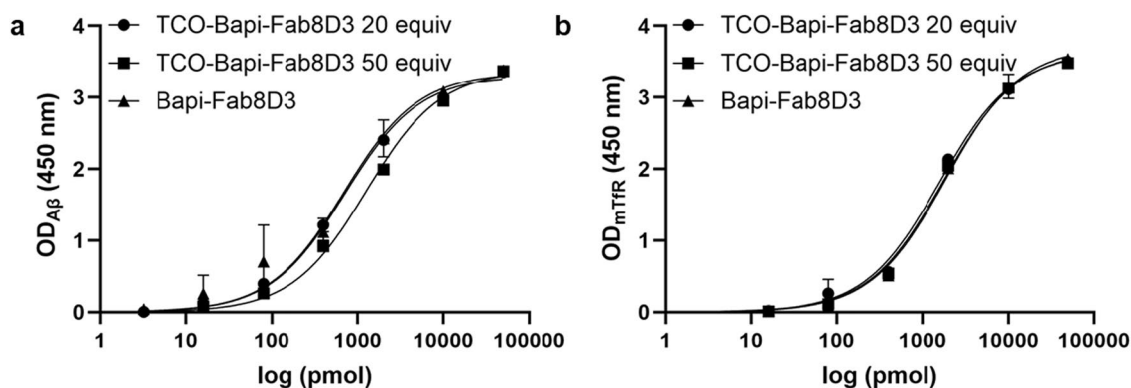


Fig. 2 ELISA results of Bapi-Fab8D3 with TCO modification. **a** Binding affinity toward amyloid- β (A β) following modification of Bapi-Fab8D3 with 20 and 50 TCO equivalents, compared to the unmodified antibody, showed retained affinity relative to the unmodified antibody. **b** Binding affinity toward the transferrin receptor (TfR) after modification with 20 and 50 TCO equivalents demonstrated preserved affinity with both modifications relative to the unmodified antibody

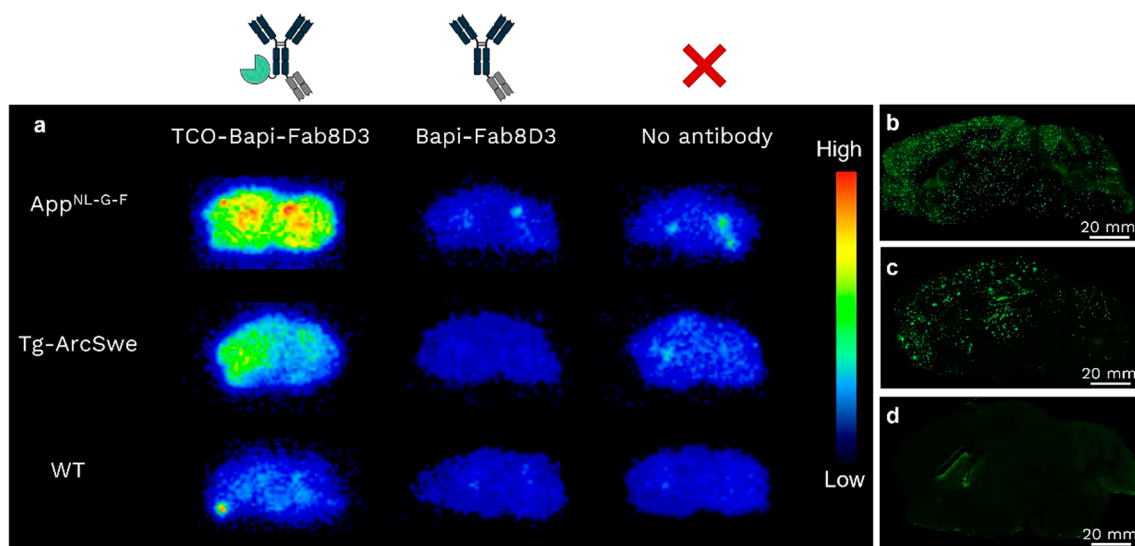


Fig. 3 TCO groups remain reactive in vivo, enabling selective signal localization to pathology-rich regions. **a** Autoradiography images of brain sections prepared from mice administered with TCO-Bapi-Fab8D3, Bapi-Fab8D3, or no antibody, after incubation with a gallium-68 radiolabeled tetrazine. Only sections prepared from mice with A β pathology (App^{NL-G-F} and Tg-ArcSwe) show retention of the tetrazine, indicating that these sections contained reactive TCO groups attached to A β -bound antibody. Mice receiving unmodified Bapi-Fab8D3 or no antibody, as well as wild-type (WT) control mice without A β pathology showed no signal. TCO, trans-cyclooctene. **b–d** Representative images of LCO-stained A β pathology in App^{NL-G-F} (**b**), Tg-ArcSwe (**c**) and WT (**d**) sagittal brain sections, respectively

differences between App^{NL-G-F} and WT mice and with improved clearance compared to earlier time points (i.e., 1.5 h) (Fig. 4b, Fig. S2). However, in saline-perfused brains, isolated after the PET scan, App^{NL-G-F} mice displayed higher ex vivo concentrations of [¹⁸F]MeTzA compared to WT controls (Fig. 4c). A similar genotype-dependent trend was also observed in the brain-to-blood concentration ratio ($P=0.13$) (Fig. 4d). This difference between App^{NL-G-F} and WT mice was not observed with [¹⁸F]HTzA. Tetrazines do not have a specific biological target in vivo, but A β plaques are known to retain certain substances due to altered tissue composition. Therefore, the observed difference may reflect non-specific retention of [¹⁸F]MeTzA in A β -rich brain regions. Importantly, biodistribution, including analysis of skull uptake demonstrated no genotype-dependent differences in tracer distribution (Fig. 4e, Fig. S3), indicating that tetrazine metabolism did not differ between App^{NL-G-F} and WT mice. Moreover, comparable skull radioactivity was observed for [¹⁸F]HTzA and [¹⁸F]MeTzA, suggesting a similar extent of defluorination between tracers. Given the potential non-specific in vivo binding of [¹⁸F]MeTzA and the higher reactivity of HTzs[37], only [¹⁸F]HTzA was selected for further use in pretargeted PET imaging studies.

Pharmacokinetics of DOTA-PEG₁₁-Tz

DOTA-PEG₁₁-Tz exhibited very low brain concentrations (Fig. S4a), and was able to react with TCOs in plasma (Fig. S4b), indicating its suitability for subsequent pretargeted PET studies to quench circulating TCOs without affecting those within the brain.

Pretargeted PET imaging with [¹⁸F]HTzA and TCO-Bapi-Fab8D3 reveals A β pathology

App^{NL-G-F} and WT mice were administered with TCO-Bapi-Fab8D3 containing an average of 9 TCOs per antibody. As a control, a group of App^{NL-G-F} mice received unmodified Bapi-Fab8D3. PET imaging three days later at 3.5–4.5 h post [¹⁸F]HTzA administration revealed that the App^{NL-G-F} mice that had received TCO-Bapi-Fab8D3 showed a higher brain signal compared to both WT mice injected with TCO-Bapi-Fab8D3 and App^{NL-G-F} mice that received only the unmodified antibody (Fig. 5a). Both App^{NL-G-F} and WT mice administered with TCO-Bapi-Fab8D3 displayed an elevated signal in the outer regions of the brain, indicating that [¹⁸F]HTzA reacted with TCOs in these areas, resulting in some spill-in to the brain parenchyma. To visualize differences in brain concentrations between App^{NL-G-F} and WT mice, excluding the contribution from this peripheral spill-in, a subtraction image was generated to isolate the signal originating specifically from A β targeting (Fig. 5b). Brain uptake was further quantified in AD-relevant

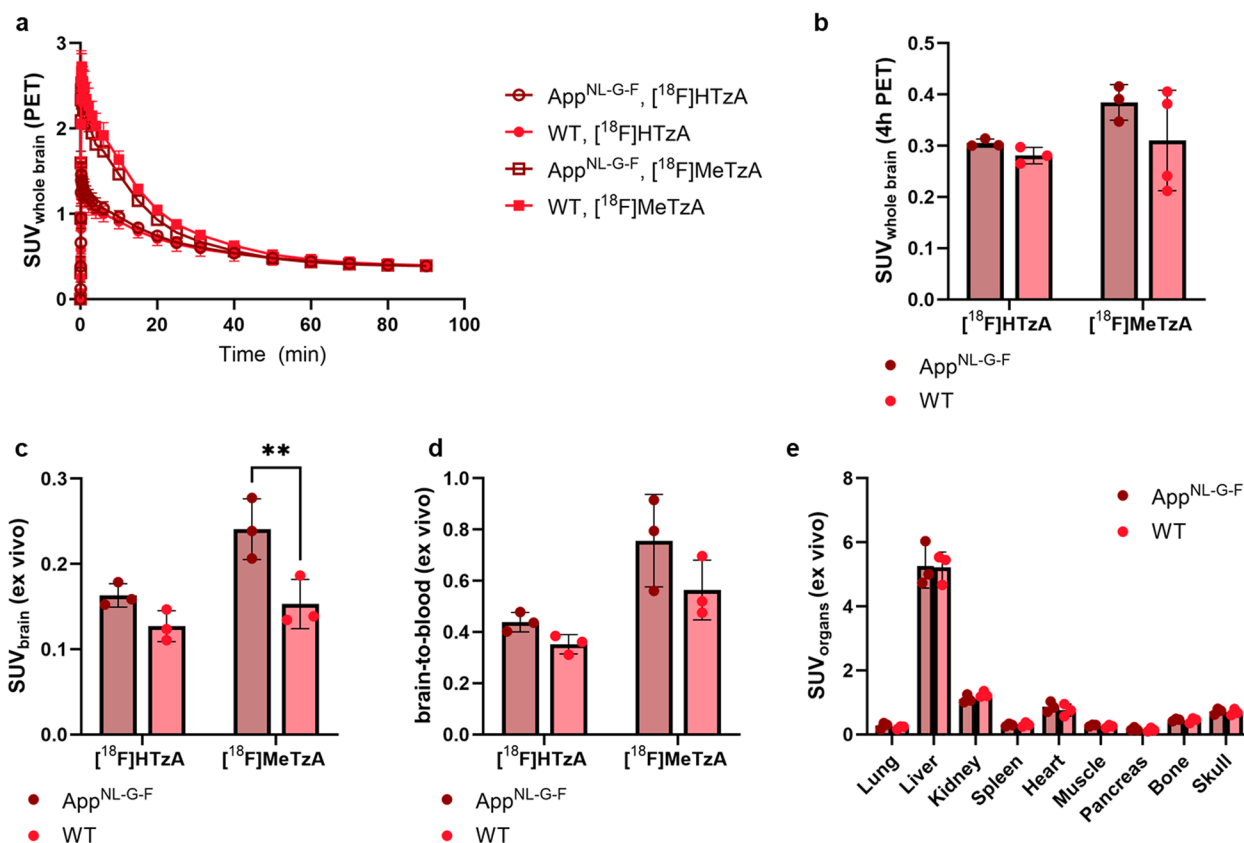


Fig. 4 Brain concentrations of two fluorine-18 (¹⁸F)-tetrazines. **a** In vivo brain concentrations of [¹⁸F]HTzA and [¹⁸F]MeTzA, expressed as SUV, in App^{NL-G-F} and wild-type (WT) mice over the 90-min scanning period. **b** In vivo brain concentrations, expressed as SUV, at 4 h post administration of [¹⁸F]HTzA or [¹⁸F]MeTzA in App^{NL-G-F} and WT mice. **c** Ex vivo measured concentrations, expressed as SUV at 5 h post administration, in perfused isolated brain after PET scanning in App^{NL-G-F} and WT mice. **d** Ex vivo brain-to-blood concentration ratio at 5 h post administration in App^{NL-G-F} and WT mice. **e** Ex vivo concentrations in selected peripheral organs at 5 h post administration of [¹⁸F]HTzA in App^{NL-G-F} and WT mice. Mean ± SD of $n=3$ for HTzA per genotype and $n=2$ for MeTzA per genotype (**a**); mean ± SD of $n=3$ per condition, except for WT [¹⁸F]MeTzA where $n=4$ (**b**); mean ± SD of $n=3$ per condition (**c–e**). ** $P < 0.01$, two-way ANOVA Sidak's multiple comparison (**b–e**). SUV, standardized uptake value, a dose- and weight-normalized concentration

deep brain regions (hippocampus and thalamus) using PET (Fig. 5c), in the whole brain via ex vivo γ -counting of perfused and isolated brain tissue (Fig. 5d), and in relation to terminal [¹⁸F]HTzA blood concentrations (Fig. 5e). We additionally assessed systemic biodistribution (Fig. 5f), which confirmed that the main peripheral accumulation occurred in the liver followed by the kidneys. No increased retention was observed in spleen, which has a high TfR expression, suggesting that the rate of click reaction between the tetrazine and the TCO-antibody in peripheral TfR-expressing tissues is limited. Across all outcome measures, the App^{NL-G-F} mice that had received TCO-Bapi-Fab8D3 retained more [¹⁸F]HTzA than both WT mice (30% more in the hippocampus, 38% in the thalamus, 86% in whole brain ex vivo, and 81% in the brain-to-blood ratio) and App^{NL-G-F} mice that received unmodified Bapi-Fab8D3 (43% more in the hippocampus, 37% in the thalamus, 48% in whole brain

ex vivo, and 64% in the brain-to-blood ratio). Furthermore, no significant differences were observed between WT mice administered with TCO-Bapi-Fab8D3 (lacking A β pathology) and App^{NL-G-F} mice that received unmodified Bapi-Fab8D3 (lacking the TCO handle). In addition, the radioactivity in these mice was very similar to that seen in antibody naïve mice, indicating similar results for all the control mice (Fig. 4). Taken together, these results demonstrate the successful in vivo PET imaging of A β pathology using the pretargeted approach.

Confirmation of A β pathology

The presence of A β was confirmed in all App^{NL-G-F} mice used in the pretargeted PET study. A β levels did not differ between animals that received TCO-Bapi-Fab8D3 and those that received unmodified Bapi-Fab8D3 (Fig. S5).

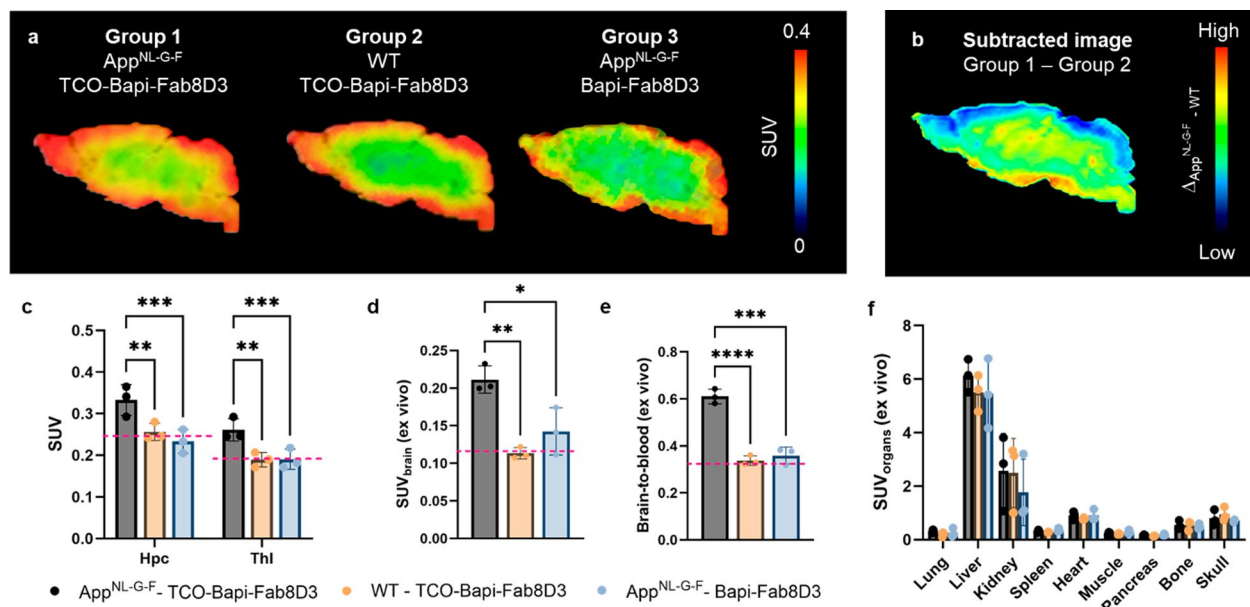


Fig. 5 Pretargeted imaging of brain A β . **a** Group-averaged sagittal PET images based on activity measured at 3.5–4.5 h post [^{18}F]HTzA administration in App^{NL-G-F} and WT mice that had received TCO-Bapi-Fab8D3, and in App^{NL-G-F} mice that had received unmodified Bapi-Fab8D3. The most intense signal was obtained in App^{NL-G-F} mice receiving TCO-Bapi-Fab8D3. **b** An image representing the signal difference between App^{NL-G-F} and WT mice that had received TCO-Bapi-Fab8D3 to illustrate the difference between these groups. **c** Brain radioactivity concentration based on PET imaging, expressed as SUV, in the hippocampus (Hpc) and thalamus (Thl) in App^{NL-G-F} and WT mice that had received TCO-Bapi-Fab8D3, and App^{NL-G-F} mice that had received unmodified Bapi-Fab8D3. **d** Brain radioactivity concentration, expressed as SUV, in perfused isolated brain after PET scanning in App^{NL-G-F} and WT mice that had received TCO-Bapi-Fab8D3, and in App^{NL-G-F} mice that had received Bapi-Fab8D3. **e** Ex vivo brain-to-blood concentration ratio after PET scanning in App^{NL-G-F} and WT mice that had received TCO-Bapi-Fab8D3, and in App^{NL-G-F} mice that had received Bapi-Fab8D3. **f** Radioactivity concentrations in peripheral organs, expressed as SUV, after PET scanning in App^{NL-G-F} and WT mice that had received TCO-Bapi-Fab8D3, and in App^{NL-G-F} mice that had received Bapi-Fab8D3. Average images based on $n=3$ per group (**a**); difference between average images of App^{NL-G-F} and WT mice (**b**); Mean \pm SD of $n=3$ per condition (**c–e**). The red lines in **c–e** represent concentrations of [^{18}F]HTzA in antibody naïve mice. * $P < 0.05$, ** $P < 0.01$, *** $P < 0.001$, **** $P < 0.0001$. Two-way ANOVA Sidak’s multiple comparison (**c**), one-way ANOVA Tukey’s multiple comparison (**d, e**). SUV, standardized uptake value

Discussion

PET imaging of the brain using a pretargeted approach has been proposed as a promising strategy to enable the use of antibody-based radioligands labeled with short-lived, clinically relevant radionuclides such as ^{18}F [16–18, 20]. The use of antibodies instead of small molecule-based radioligands would enable the visualization and quantification of intrabrain protein targets for which no radioligands are currently available, thereby unlocking transformative potential for molecular imaging in neurology.

Despite its promise, pretargeted PET imaging of brain targets has not been successfully implemented until now. One major challenge lies in the need to combine highly brain-penetrant antibodies with tetrazines that possess suitable pharmacokinetic properties; specifically, rapid brain entry and clearance. Without this fine-tuned balance, sufficient imaging contrast cannot be achieved [38]. A recent study demonstrated an alternative version of the pretargeted approach using intrathecally delivered

antisense oligonucleotides (ASOs) modified with tetrazine, followed by PET imaging with an ^{18}F -labeled TCO [18]. While elegant in concept, this strategy involves an invasive procedure, with ASO-tetrazine delivered via the cisterna magna. In contrast, delivering the pretargeting agent across the BBB provides a more physiologically relevant and less invasive method to reach targets throughout the entire brain parenchyma. Another recent study, currently available only as a preprint, employed a strategy similar to the one presented here [39]. It used a bispecific antibody (biAb) targeting both A β and the TfR, and reported increased brain retention of an ^{18}F -labeled tetrazine in TCO-biAb-treated AD model mice compared to similarly treated WT mice. However, that study lacked key control groups, specifically, A β -expressing mice that were not injected with antibody and mice treated with the unmodified biAb, making it difficult to assess the specificity of the tetrazine retention. Our results underscore the importance of including such controls, as retention of radiolabeled tetrazines in A β -rich tissue can occur independently of specific TCO conjugation, potentially

confounding the interpretation of imaging specificity. In addition, by including tetrazine-only (no antibody administration) and unmodified antibody controls, and by demonstrating comparable skull uptake across genotypes, we confirm that neither non-specific tetrazine accumulation nor defluorination significantly biases the subtraction-based readout.

The bispecific antibody format used in the present study is similar to the Trontinemab antibody currently being evaluated in clinical trials by Roche. This format, which features monovalent binding to TfR, has been shown to mediate highly efficient BBB transcytosis and high accumulation at A β deposits in the brain [28, 29]. These two characteristics are likely the most important features of bispecific antibodies intended for use in a pretargeted imaging approach. We note that although TfR-mediated shuttling increases brain delivery, absolute brain uptake remains modest relative to systemic exposure. Nevertheless, the uptake achieved is sufficient for robust A β -specific PET imaging, and the low accumulation in off-target TfR-expressing organs, such as the spleen, further supports the safety of this approach. Peripheral accumulation was primarily observed in the liver and kidneys, consistent with normal clearance pathways, whereas no increased splenic retention was detected in the pretargeting experiments, likely reflecting limited formation of clicked product in peripheral TfR-expressing tissues.

In addition to the Roche-format, we have previously used other bispecific antibody formats labeled with iodine-124 for direct PET imaging of brain A β [11, 12, 35, 40–42]. In those studies, the difference in radioligand uptake between AD and WT mice was somewhat more pronounced than that observed here. These observations suggest that optimizing TCO load on the antibody could further improve the contrast in pretargeted imaging. However, it is essential to ensure that antibody affinity for both A β and TfR is maintained if higher TCO loading is applied. Previous studies have shown that excessive TCO conjugation can reduce antibody affinity and impair transcytosis across the BBB via TfR-mediated delivery. Therefore, careful optimization of TCO modification remains a key factor in maximizing imaging performance. In addition, further improvements could be achieved by refining other components of the pretargeting system. For instance, developing ^{18}F -tetrazines with enhanced brain delivery and rapid brain washout of unbound tetrazine could improve the target-to-background ratio. In our study, we compared two tetrazine variants: the more lipophilic [^{18}F]MeTzA and the more hydrophilic [^{18}F]HTzA. While [^{18}F]MeTzA initially demonstrated higher brain uptake, it accumulated to a greater extent in App^{NL-G-F} mice compared to WT controls. This suggests that its

lipophilicity may contribute to non-specific retention in A β -rich regions.

We evaluated kinetics of both tetrazines at 1.5 and 4 h post-injection and observed similar brain concentrations at the later time-point across genotypes, accompanied by increased washout after 4 h relative to 1.5 h. This supports 4 h post-injection as a suitable imaging time for maximizing contrast in the current system.

Considering these findings and the higher reactivity of [^{18}F]HTzA, we selected [^{18}F]HTzA for use in the final pretargeted imaging experiments. Nevertheless, a slightly more lipophilic [^{18}F]HTzA derivative with balanced properties could further improve the approach [17, 37]. In future work, the development of tetrazines with even faster systemic and brain clearance may enable earlier imaging time-points while maintaining high specificity.

Similarly, optimizing antibody dose and systemic clearance, either through antibody engineering or by improving the efficiency of the blocking or clearing agents, may contribute to reducing off-target binding and enhancing imaging contrast. Together, these considerations highlight both the promise of pretargeted immunoPET and the importance of continued optimization of shuttle affinity, tetrazine pharmacokinetics, and TCO loading to support translation.

Conclusions

In this study, we demonstrate successful pretargeted PET imaging of brain A β pathology using a bispecific antibody engineered for TfR-mediated transport and modified with TCO. This approach enabled the use of ^{18}F -labeled tetrazines for high-contrast imaging, overcoming limitations of poor BBB penetration and reliance on long-lived radionuclides. While the current work focused on A β , the strategy is broadly applicable to other brain targets, provided a suitable antibody is available. Further optimization of tetrazine properties and TCO loading may enhance imaging performance. Overall, this pretargeted PET methodology represents a major advance in molecular imaging, with potential for non-invasive visualization of previously inaccessible brain proteins in both research and clinical settings.

Abbreviations

^{18}F	Fluorine-18 (radionuclide)
^{68}Ga	Gallium-68 (radionuclide)
AD	Alzheimer's disease
A β	Amyloid- β
A_m	Molar activity
BBB	Blood-brain barrier
CT	Computed tomography
DMSO	Dimethylsulfoxide
ELISA	Enzyme-linked immunosorbent assays
hlgG	Human immunoglobulin G
i.p.	Intraperitoneal
i.v.	Intravenous

LCO	Luminescent Conjugated Oligothiophene
PET	Positron emission tomography
Radio-TLC	Radio-thin layered chromatography
RCY	Radiochemical yield
RCP	Radiochemical purity
SPE	Solid-phase extraction
TCO	Trans-cyclooctene
TfR	Transferrin receptor
SUV	Standardized uptake value
VOI	Volume of interest

Supplementary Information

The online version contains supplementary material available at <https://doi.org/10.1186/s40035-025-00532-2>.

Additional file 1. **Fig. S1.** Chemical structures of tetrazines used. **Fig. S2.** Brain PET concentrations at 1.5 hours and 4 hours post tracer administration of two ¹⁸F-tetrazines. **Fig. S3.** Ex vivo skull retention at 5 hours post administration of [¹⁸F]HTzA and [¹⁸F]MeTzA in App^{NL-G-F} and WT mice. **Fig. S4.** Brain concentrations of [⁶⁸Ga]Ga-DOTA-PEG₁₁-Tz. **Fig. S5.** Amyloid-β (Aβ) levels in the brains of mice included in the pretargeted PET study. **Table S1.** Mice used in the different studies.

Additional file 2: Uncropped radioTLC.

Acknowledgements

We are grateful to Tagworks Pharmaceuticals for providing the DOTA-PEG₁₁-Tz and to Peter R Nilsson and Therese Klingstedt for providing the LCO HS-84. We would like to thank Takashi Saito and Takaomi Saïdo at RIKEN Center for Brain Science for the development of the App^{NL-G-F} model and Lars Nilsson presently at Oslo University, for the development of the Tg-ArcSwe model, used in the present study. The molecular imaging work in this study was performed at the Preclinical PET-MRI Platform, a research infrastructure at Uppsala University, Sweden.

Author contributions

Conceptualization: S.L.B., J.E., D.S. and S.S. Methodology: E.S., S.L.B., J.E., D.S., S.S., L.B. and L.O. Investigation: S.L.B., J.E., D.S., S.S. and N.B. Visualization: S.L.B. and Q.Y. Data curation: S.L.B., D.S. and S.S. Funding acquisition: S.L.B., D.S. and S.S. Writing—original draft: S.L.B., D.S. and S.S. Writing—review & editing: S.L.B., D.S., S.S., J.E., Q.Y., N.B., E.S., L.B. and L.O.

Funding

Open access funding provided by Uppsala University. Vetenskapsrådet (2021-01083, Stina Syvänen, 2021-03524, Dag Sehlin), Parkinsonfonden, Alzheimerfonden, Hjärnfonden, Åhlén-stiftelsen, Gun och Bertil Stohnes Stiftelse, Stiftelsen för Gamla Tjänarinnor, Tore Nilsons stiftelse, Konung Gustaf V:s och Drottning Victorias Frimurarestiftelse.

Availability of data and materials

All data are available in the main text or the supplementary materials. The datasets used and/or analyzed during the current study are available from the corresponding author on reasonable request.

Declarations

Ethics approval and consent to participate

All animal experiments described in this study were approved by the Uppsala County Animal Ethics board (5.8.18\16493/2024), following the rules and regulations of the Swedish Animal Welfare Agency and complied with the European Communities Council Directive of 22 September 2010 (2010/63/EU).

Consent for publication

Not applicable.

Competing interests

The authors declare that they have no competing interests.

Author details

¹Department of Public Health and Caring Sciences, Uppsala University, 751 85 Uppsala, Sweden. ²Department of Medicinal Chemistry, Uppsala University, 751 85 Uppsala, Sweden. ³PET Centre, Uppsala University Hospital, 751 85 Uppsala, Sweden.

Received: 29 July 2025 Accepted: 9 December 2025

Published online: 26 December 2025

References

- Mukherjee A, Biswas S, Roy I. Immunotherapy: an emerging treatment option for neurodegenerative diseases. *Drug Discov Today*. 2024;29:103974.
- Schwartz M. Can immunotherapy treat neurodegeneration? *Science*. 2017;357:254–5.
- van Dyck CH, Swanson CJ, Aisen P, Bateman RJ, Chen C, Gee M, et al. Lecanemab in early Alzheimer's disease. *N Engl J Med*. 2023;388:9–21.
- Honig LS, Sabbagh MN, van Dyck CH, Sperling RA, Hersch S, Matta A, et al. Updated safety results from phase 3 lecanemab study in early Alzheimer's disease. *Alzheimers Res Ther*. 2024;16(1):105.
- Chapleau M, Iaccarino L, Soleimani-Meigooni D, Rabinovici GD. The role of amyloid PET in imaging neurodegenerative disorders: a review. *J Nucl Med*. 2022;63:135–195.
- Ni R, Gillberg P-G, Bergfors A, Marutle A, Nordberg A. Amyloid tracers detect multiple binding sites in Alzheimer's disease brain tissue. *Brain*. 2013;136:2217–27.
- Gouilly D, Saint-Aubert L, Ribeiro M-J, Salabert A-S, Tauber C, Péran P, et al. Neuroinflammation PET imaging of the translocator protein (TSPO) in Alzheimer's disease: an update. *Eur J Neurosci*. 2022;55:1322–43.
- Mathis CA, Lopresti BJ, Ikonovic MD, Klunk WE. Small-molecule PET tracers for imaging proteinopathies. *Semin Nucl Med*. 2017;47:553–75.
- Smith R, Capotosti F, Schain M, Ohlsson T, Vokali E, Molette J, et al. The α-synuclein PET tracer [¹⁸F] ACI-12589 distinguishes multiple system atrophy from other neurodegenerative diseases. *Nat Commun*. 2023;14:6750.
- Korat S, Bidesi NSR, Bonanno F, Di Nanni A, Hoàng ANN, Herfert K, et al. Alpha-synuclein PET tracer development—an overview about current efforts. *Pharmaceuticals (Basel)*. 2021;14(9):847.
- Bonvicini G, Syvänen S, Andersson KG, Haaparanta-Solin M, López-Picón F, Sehlin D. ImmunoPET imaging of amyloid-beta in a rat model of Alzheimer's disease with a bispecific, brain-penetrating fusion protein. *Transl Neurodegener*. 2022;11:1–14.
- Sehlin D, Fang XT, Cato L, Antoni G, Lannfelt L, Syvänen S. Antibody-based PET imaging of amyloid beta in mouse models of Alzheimer's disease. *Nat Commun*. 2016;7:1–11.
- Hultqvist G, Syvänen S, Fang XT, Lannfelt L, Sehlin D. Bivalent brain shuttle increases antibody uptake by monovalent binding to the transferrin receptor. *Theranostics*. 2017;7:308–18.
- Baghirov H. Mechanisms of receptor-mediated transcytosis at the blood-brain barrier. *J Control Release*. 2025;381:113595.
- Sehlin D, Hultqvist G, Michno W, Aguilar X, Dahlén AD, Cerilli E, et al. Bispecific brain-penetrant antibodies for treatment of Alzheimer's disease. *J Prev Alzheimers Dis*. 2025;12(8):100214.
- van den Lopes Broek S, Shalgunov V, García Vázquez R, Beschornor N, Bidesi NSR, Nedergaard M, et al. Pretargeted imaging beyond the blood-brain barrier—utopia or feasible? *Pharmaceuticals*. 2022;15:1–15.
- Shalgunov V, van den Lopes Broek S, Vang Andersen I, García Vázquez R, Raval NR, Palmer M, et al. Pretargeted imaging beyond the blood-brain barrier. *RSC Med Chem*. 2022;14:444–53.
- Cook BE, Pickel TC, Nag S, Bolduc PN, Beshr R, Forsberg Morén A, et al. PET imaging of antisense oligonucleotide distribution in rat and nonhuman primate brains using click chemistry. *Sci Transl Med*. 2025;17(797):eadl1732.
- Rossin R, Robillard MS. Pretargeted imaging using bioorthogonal chemistry in mice. *Curr Opin Chem Biol*. 2014;21:161–9.
- Stéen EJJ, Edem PE, Nørregaard K, Jørgensen JT, Shalgunov V, Kjaer A, et al. Pretargeting in nuclear imaging and radionuclide therapy: improving efficacy of theranostics and nanomedicines. *Biomaterials*. 2018;179:209–45.

21. Goldenberg DM, Sharkey RM, Paganelli G, Barbet J, Chatal JF. Antibody pretargeting advances cancer radioimmunodetection and radioimmunotherapy. *J Clin Oncol*. 2006;24(5):823–34.
22. Saito T, Matsuba Y, Mihira N, Takano J, Nilsson P, Itohara S, et al. Single App knock-in mouse models of Alzheimer's disease. *Nat Neurosci*. 2014;17:661–3.
23. Philipson O, Hammarström P, Nilsson KPR, Portelius E, Olofsson T, Ingelsson M, et al. A highly insoluble state of A β similar to that of Alzheimer's disease brain is found in Arctic APP transgenic mice. *Neurobiol Aging*. 2009;30:1393–405.
24. Zielinski M, Peralta Reyes FS, Gremer L, Schemmert S, Frieg B, Schäfer LU, et al. Cryo-EM of A β fibrils from mouse models find tg-APP^{Arctic} fibrils resemble those found in patients with sporadic Alzheimer's disease. *Nat Neurosci*. 2023;26:2073–80.
25. Salloway S, Sperling R, Fox NC, Blennow K, Klunk W, Raskind M, et al. Two phase 3 trials of bapineuzumab in mild-to-moderate Alzheimer's disease. *N Engl J Med*. 2014;370(4):322–33.
26. Kissel K, Hamm S, Schulz M, Vecchi A, Garlanda C, Engelhardt B. Immunohistochemical localization of the murine transferrin receptor (TfR) on blood-tissue barriers using a novel anti-TfR monoclonal antibody. *Histochem Cell Biol*. 1998;110:63–72.
27. Schlein E, Andersson KG, Dallas T, Syvänen S, Sehlin D. Reducing neonatal Fc receptor binding enhances clearance and brain-to-blood ratio of TfR-delivered bispecific amyloid- β antibody. *MAbs*. 2024;16:1–11.
28. Grimm HP, Schumacher V, Schäfer M, Imhof-Jung S, Freskgård P-O, Brady K, et al. Delivery of the Brainshuttle™ amyloid-beta antibody fusion trontinemab to non-human primate brain and projected efficacious dose regimens in humans. *MAbs*. 2023;15:1–14.
29. Niewoehner J, Bohrmann B, Collin L, Ulrich E, Sade H, Maier P, et al. Increased brain penetration and potency of a therapeutic antibody using a monovalent molecular shuttle. *Neuron*. 2014;81:49–60.
30. Dahlén AD, Roshanbin S, Aguilar X, Bucher NM, van den Lopes Broek S, Sehlin D, et al. PET imaging of TREM2 in amyloid-beta induced neuroinflammation. *Eur J Nucl Med Mol Imaging*. 2025;52:4320–33.
31. Syvänen S, Fang XT, Faresjö R, Rokka J, Lannfelt L, Olberg DE, et al. Fluorine-18-labeled antibody ligands for PET imaging of amyloid- β in brain. *ACS Chem Neurosci*. 2020;7:1–16.
32. Schlein E, van den Lopes Broek S, Dallas T, Andersson KG, Syvänen S, Eriksson J, et al. Fluorine-18 immunoPET imaging of antibody brain kinetics and amyloid-beta pathology. *ACS Pharmacol Transl Sci*. 2025;8(8):2804–13.
33. Faresjö R, Sehlin D, Syvänen S. Age, dose, and binding to TfR on blood cells influence brain delivery of a TfR-transported antibody. *Fluids Barriers CNS*. 2023;20:1–17.
34. Klingstedt T, Shirani H, Parvin F, Nyström S, Hammarström P, Graff C, et al. Dual-ligand fluorescence microscopy enables chronological and spatial histological assignment of distinct amyloid- β deposits. *J Biol Chem*. 2025;301(1):108032.
35. Meier SR, Sehlin D, Roshanbin S, Falk VL, Saito T, Saido TC, et al. 11C-PiB and 124I-antibody PET provide differing estimates of brain amyloid- β after therapeutic intervention. *J Nucl Med*. 2022;63(2):302–9.
36. Dahlén AD, Roshanbin S, Bucher NM, Sehlin D, Syvänen S. Evaluating the impact of age and treatment on neuroinflammation-related proteins in mouse models of proteinopathies. *Exp Neurol*. 2026;395:115475.
37. Stéen E, Jørgensen JT, Denk C, Battisti UM, Nørregaard K, Edem PE, et al. Lipophilicity and click reactivity determine the performance of bioorthogonal tetrazine tools in pretargeted *in vivo* chemistry. *ACS Pharmacol Transl Sci*. 2021;4(2):824–33.
38. Bredack C, Edelmann MR, Borroni E, Gobbi LC, Honer M. Antibody-based *in vivo* imaging of central nervous system targets-evaluation of a pretargeting approach utilizing a TCO-conjugated brain shuttle antibody and radiolabeled tetrazines. *Pharmaceuticals (Basel)*. 2022;15(12):1445.
39. Gustavsson T, Kustermann T, Hvass L, Shalgunov V, Skovsbo Clausen A, Stotz S, et al. Brain pretargeted PET - new horizons to image CNS targets with monoclonal antibodies. *bioRxiv* 2024.10.12.617694
40. Meier SR, Syvänen S, Hultqvist G, Fang XT, Roshanbin S, Lannfelt L, et al. Antibody-based *in vivo* PET imaging detects amyloid- β reduction in Alzheimer transgenic mice after BACE-1 inhibition. *J Nucl Med*. 2018;59(12):1885–91.
41. Fang XT, Hultqvist G, Meier SR, Antoni G, Sehlin D, Syvänen S. High detection sensitivity with antibody-based PET radioligand for amyloid beta in brain. *Neuroimage*. 2019;184:881–8.
42. Sehlin D, Fang XT, Meier SR, Jansson M, Syvänen S. Pharmacokinetics, biodistribution and brain retention of a bispecific antibody-based PET radioligand for imaging of amyloid- β . *Sci Rep*. 2017;7:17254.